Fatigue strength improvement of linear friction welded butt joints of low carbon steel by pressurizing after oscillation

Huilin Miao[1,*], Seiichiro Tsutsumi[2], Takayuki Yamashita[1], Yoshiaki Morisada[1], Hidetoshi Fujii[1,*]

[1] *Joining and Welding Research Institute, Osaka University, Osaka 567-0047, Japan*
[2] *Graduate School of Engineering, Osaka University, Osaka 565-0871, Japan*

Abstract: Although linear friction welding (LFW) has received significant attention as an effective solid-state welding method, the fatigue properties of LFW joints have not been fully investigated. In this study, the fatigue strength of the steel joints fabricated using LFW was investigated and improved by increasing the pressure after oscillation. Low-carbon steel SM490A was successfully joined using LFW without unbonded areas or apparent softening in the heat-affected zone (HAZ). The microhardness, microstructure, weld toe shape, and fatigue life were assessed to investigate their relationships with the pressure conditions after oscillation. The results indicated that increasing the pressure after oscillation improved the area fraction of martensite (M) and the hardness of the weld interface center. The weld toe radius (ρ) and weld toe angle (α) also increased regardless of the upset control condition. The increasing of the pressure after oscillation from 50 MPa to 300 MPa increased ρ from 0.4 mm to 2.1 mm and the α increased from 92.7° to 103.4° at the weld center, accompanied by a reduced stress concentration factor (K_t) from 3.0 to 1.7. Under the fatigue test conditions of the stress range of 380 MPa, the fatigue life of the LFW as-welded joints was increased by approximately 31% when the pressure after oscillation was 250 MPa compared to that of 50 MPa and by 87% when it was 300 MPa compared to that of 250 MPa. Despite the possibility of fracture initiation at the weld toe at the edge of the LFW joints, the fatigue strength demonstrated a substantially longer fatigue life than the *S-N* design curve FAT90 recommended by the International Institute of Welding.

Keywords: Linear friction welding, Fatigue strength, Weld toe radius

* Corresponding author, E-mail: miao@jwri.osaka-u.ac.jp (H. Miao),fujii@jwri.osaka-u.ac.jp (H. Fujii)

1. Introduction

Linear friction welding (LFW) is a solid-state process that joins similar or dissimilar materials without any filler material or external heat sources [1–5]. This involves applying high-frequency oscillations to workpieces in a linear motion under applied pressure, resulting in heat generation at the interface between the two parts [6, 7]. The LFW process can be divided into four stages [8–11]: the contact stage (stage 1), during which the reciprocating and stationary components contact each other under a load; the pressurization and temperature rising stage (stage 2), during which the stationary component is forced against the reciprocating component, which shows a reciprocating motion in a linear direction; the deformation stage (stage 3), during which the weld interface is plasticized and expelled as a flash; and the cooling stage (stage 4), during which the oscillation motion is stopped, and a forge force is applied to produce a consolidated joint. Moreover, in LFW, the softened material is expelled from the joint interface as a flash, similar to rotary friction welding [12]. The volume of the flash is controlled by the upset. In the LFW, the total upset includes part of the oscillation process (stage 3) and the pressurizing process after the oscillation (stage 4). LFW offers several advantages over other welding techniques. First, LFW is highly energy efficient because only frictional heat is required to create a joint. Second, it can be applied to objects that are not axially symmetric, whereas conventional rotary friction welding is suitable only for cylindrical objects [9]. Additionally, LFW does not require a tool, whereas friction stir welding is limited by tool life expectancy. Therefore, LFW is considered an appropriate approach for manufacturing aerospace components, such as bladed disks [13–16]. Arc welding of butt joints of steel plates can be more challenging than LFW because full penetration requires beveling the plates to a V-groove. The intrinsic properties of the arc welding process result in inferior mechanical properties of the welded joints owing to high welding temperatures and rapid temperature changes. However, the LFW welding process can be completed within a few seconds without preparing the V-groove because of the complete contact between the two specimens. As the LFW welding temperature is lower than the melting point of steel, the inferior mechanical properties caused by the high welding temperature during fusion welding can be improved. Therefore, if LFW could be used to join steel structures, it would be safer and more reliable. Some reports exist on LFW steel joints based on simulations and experiments [8, 17, 18]. Although steel joints can be obtained using LFW, the fatigue properties must be considered in practical structures because cyclic loading over an extended period can cause cracks and structural failure [19]. Several studies have been conducted on the fatigue properties of LFW joints [20–25]. However, the research on the LFW fatigue tests mentioned above was carried out by removing the flash, which excluded the shape factor and reduced the stress concentration.

Several factors affect the fatigue properties of joints, such as the loading conditions [26], HAZ softness [27], mechanical properties of the material [28], microstructure [29, 30], and weld toe profile [31–33]. Owing to the stress concentration and HAZ softness, the arc welding area is a critical crack initiation area despite several techniques that can improve the weld toe radius, such as grinding [34] and tungsten inert gas dressing [35, 36]. However, removing the flash from large structures such as bridges can be labor-intensive and time-consuming, especially if joints are difficult to access. By leaving the flash in place or with less treatment, the welding process can be completed more quickly and at a lower cost. In addition, the LFW pressurization process after oscillation may change the shape of the weld by applying plastic deformation. Therefore, it is expected that the stress concentration [37], welding quality [38], and resultant fatigue life can be adjusted by modifying the flash and weld toe shape [25, 31–33]. Although some reports have separately controlled the pressures during and after oscillation [13, 39], a systematic analysis of the applied pressure on LFW after oscillation has not yet been conducted. The relationship between the weld toe shape, fatigue strength, microstructure, and applied pressure after oscillation remains unclear. Therefore, the purpose of this study

was to systematically investigate the hardness distribution, microstructure, fracture characteristics, and weld toe shape of LFW joints by increasing the pressure after oscillation.

2. Experimental procedures

Low-carbon SM490A was used in this study because it is a readily available steel grade. Additionally, SM490A is typically used for welded structures such as bridge architecture and other engineering structures. This steel plate's fatigue properties are important in understanding the application of LFW to structures. **Table 1** lists the chemical composition of the test steel. The base metal (BM) microstructure consisted of ferrite (F) and pearlite (P), as shown in **Fig. 1**. Two workpieces with dimensions of 54 mm × 40 mm × 9 mm were joined using LFW in the configuration of the butt joints. Before welding, a 40 mm × 9 mm surface was used as the joining surface, and the black oxidation layer was removed using a milling machine.

Fig. 2 shows the LFW equipment and a schematic illustration of the specimen in both the oscillation and forging directions. The loading direction (LD), oscillation direction (OD), and normal direction (ND) of the specimens during joining are shown in Fig. 2. **Table 2** lists the welding conditions used in this study. LFW was conducted at a constant amplitude of ±1.5 mm and a frequency of 50 Hz. A pressure of 50 MPa was applied during the oscillation to achieve a higher temperature [8]. Increasing the temperature of the bonding interface is believed to raise the temperature of the surrounding region and clarify the behavior of the plastic deformation zone when pressure is applied after oscillation. In contrast, pressures were maintained or adjusted to 50, 250, and 300 MPa, respectively, for a holding time of 10 s. The joints obtained under each welding condition are hereafter referred to as the 50→50MPa, 50→250MPa, and 50→300MPa joints. The welding processes were carried out using upset control, which involved controlling the displacement after contact with the samples. In this study, a constant final upset condition was used to adjust the deformation length between the two specimens to investigate the effect of the pressure after oscillation on the weld toe shape. The upsets in the oscillation process were changed and adjusted, including 3.4 mm for the 50→50MPa, 2.5 mm for 50→250MPa, and 2.0 mm for the 50→300MPa joints, respectively. The final upset value was maintained at 3.4 mm with a variation from −0.15 mm to 0 mm. This variation is because of the slight deviation in the upset caused by the post-oscillation pressurization, which is difficult to avoid compared to the upset caused by oscillation. Additionally, to check whether the upset value of the oscillation affected the weld toe shape, the weld toe shape was investigated again for the joints fabricated under the condition of a constant oscillation upset of 2.0 mm.

Cross-sectional specimens were prepared using an electric discharge machine (EDM) and cut from the obtained joint, as illustrated in **Fig. 3(a)**, where the observation position was close to the center area in the ND. The specimens underwent mechanical polishing using abrasive papers of 240 grit to 4000 grit, followed by 3 μm and 1 μm diamond paste finish. The specimen was chemically etched in a 1.5% nital solution for 8 s at room temperature, and its microstructure was observed using a scanning electron microscope (SEM). In addition, a Vickers hardness test was performed on the cross-section specimen using a load of 0.98 N at 200 μm intervals along the forging directions (see Fig. 3(a)) for a dwell time of 15 s.

Fatigue tests were conducted on nine specimens, consisting of six LFW as-welded butt joints and three BM specimens. **Fig. 3(b)** shows the geometric shapes of the BM specimens used in the fatigue tests. Polished BM specimens were used in this study to determine the fatigue properties of the BM without the effect of stress concentration. The size of the BM fatigue test specimens used in this study was similar to the length, width, and thickness of the LFW as-welded joints. An arc shape was cut by EDM in the center to avoid fracture at the clamping area with stress concentration in the fatigue test and to achieve fracture near the center of the BM specimen, thus eliminating the effect of the shape factor. Three BM specimens were polished with a 2000 grit abrasive paper before the tests. These fatigue tests were carried out at the final

upset of the 3.4 mm condition because this condition could ensure a consistent joint length and eliminate the effect of weld length on fatigue strength. A hydraulic fatigue testing machine was used with a loading frequency of 7 Hz and a stress ratio of R = 0.05. The fatigue test was defined as running out when the number of loading cycles exceeded 2×10^6. Finally, the fractured surfaces of the LFW joints were observed using a wide-area 3D measurement microscope. Moreover, to evaluate the weld toe shape quantitatively, the weld geometry and profiles of LFW joints were measured to assess the weld toe radius (ρ) and the weld toe angle (α) using the macroscope, as shown in **Fig. 4(a)**. The ρ was obtained by measuring the distance between the tangent line of the curved surface and the center of the circle. The α was obtained as the angle between the tangent lines of the curved surface. Based on the ρ and α, the K_t values were calculated and evaluated. The flash and weld toe profiles of the LFW joints were measured at three positions, namely one at the center of the specimen width and two on the sides, which were approximately 17 mm away from the center, as shown in **Fig. 4(b)**.

Table 1 Chemical composition of low carbon steel (wt.%).

Material	C	Si	Mn	P	S	Nb	V
SM490 A	0.100	0.290	1.320	0.010	0.002	0.012	0.003

Table 2 LFW conditions of this study.

Parameter		Conditions
Applied pressure during oscillation (MPa)		50
Pressure after oscillation (MPa)		50, 250, 300
Ramp time after oscillation (s)		0.01
Pressurizing time after oscillation (s)		10
Amplitude (mm)		±1.5
Frequency (Hz)		50
Upset control	Constant final upset (mm)	3.4
	Constant oscillation upset (mm)	2.0

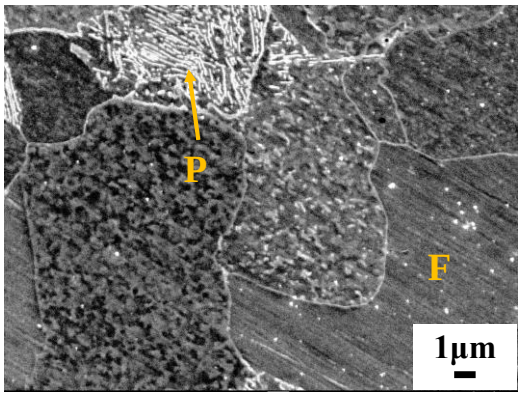

Fig. 1. SEM micrograph of the BM.

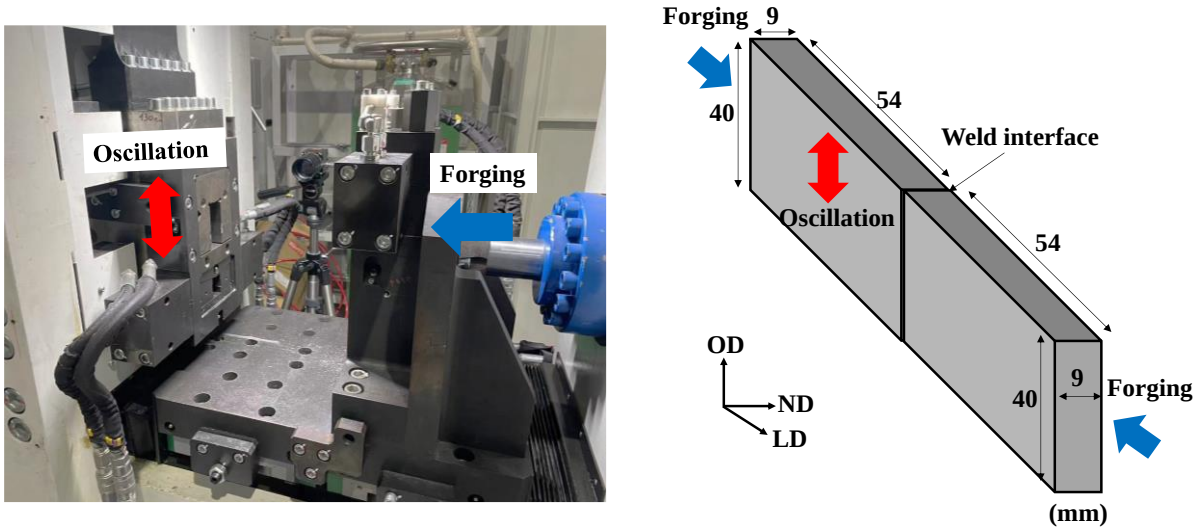

Fig. 2. Appearance of the equipment for the LFW and schematic illustration of the specimen.

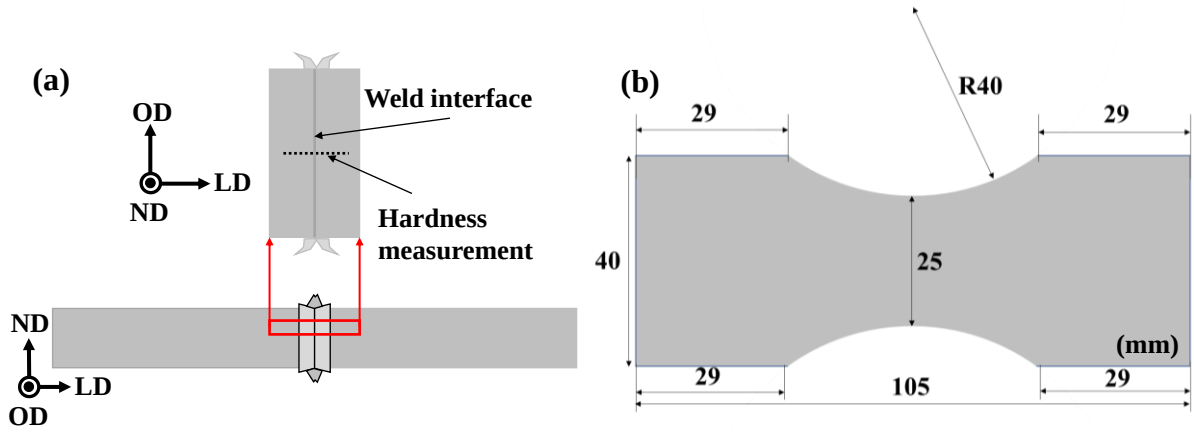

Fig. 3. Schematic illustrations: (a) Sampling of microstructure observation and hardness test; (b) Fatigue specimens for the BM.

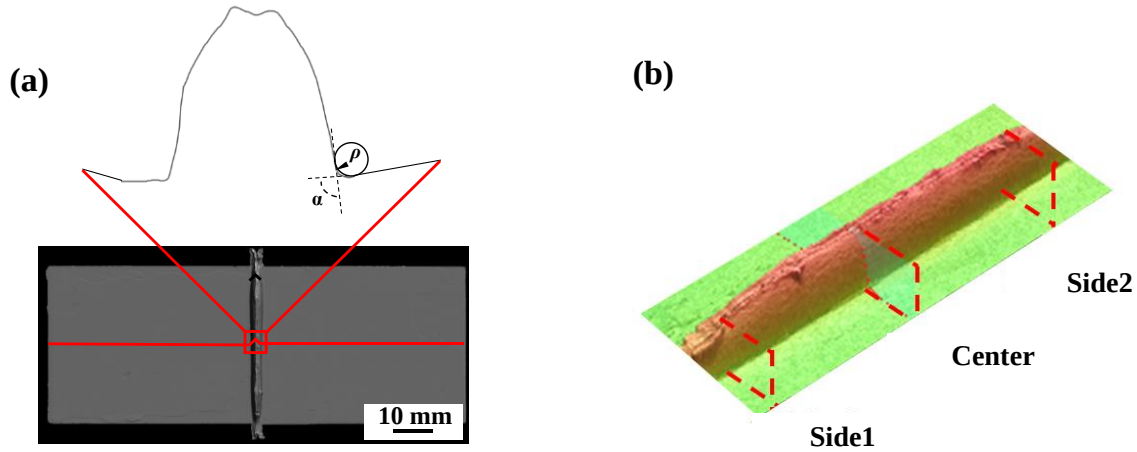

Fig. 4. (a) Definition of weld toe radius and weld toe angle, the horizontal line is parallel line of measurement; (b) Measurement locations for the weld toe shape.

3. Results

3.1. Microhardness distribution and microstructure characteristics

Fig. 5(a) shows a photograph of the 50→50MPa joint under the constant final upset condition, which serves as an example of a LFW joint. Flash discharges were observed in both the oscillation and forging directions at the joints. However, despite this, no cracks were observed in the joint, and it was considered to be sound. As shown schematically in Fig. 3(a), a specimen was obtained from the joint for microstructural observation and hardness testing.

Fig. 5(b) shows the hardness distributions of the 50→50MPa, 50→250MPa, and 50→300MPa joints along the forging direction. There was no significant difference in hardness between the oscillation and forging sides. The BM had a hardness of approximately 184 HV. A hardness peak was observed at the center of the joint under all pressure conditions. As the pressure after the oscillation increased from 50 to 250 MPa, the peak hardness value rose from 302 to 446 HV. The peak hardness value increased from 446 to 478 HV as the pressure after the oscillation increased from 250 to 300 MPa. Furthermore, no distinct softened regions were identified compared to the BM. This suggests that the LFW joints exhibit improved mechanical properties.

Fig. 6 depicts SEM micrographs of the welding interfaces of the 50→50MPa, 50→250MPa, and 50→300MPa joints at both the edge and center areas. The microstructure of BM is shown in Fig. 1. **Fig. 6(a)–(c)** show the microstructures in the middle of the weld interface. In the 50→50MPa joint, a microstructure consisting of F, bainite (B), and M was observed, as shown in Fig. 6(a). As the pressure after the oscillation increased from 50 to 250 MPa, a more significant area fraction of M was confirmed for the 50→250MPa joint, as shown in Fig. 6(b). Furthermore, for the 50→300MPa joint in Fig. 6(c), most of the microstructure consisted of laths M. This microstructure formation is related to the increase in hardness, as shown in Fig. 5(b). **Fig. 6(d)–(f)** show the microstructures at the edge of the weld interface under various pressures after oscillation. The F, B, and M microstructures were confirmed for the 50→50MPa joint, as shown in Fig. 6(d). Additionally, a significant area fraction of M was confirmed for the 50→250MPa joint, as shown in Fig. 6(e), compared to Fig. 6(d). Furthermore, a larger area of M formation was observed compared to the middle, suggesting the possibility that the cooling rate was faster at the edges than in the middle area [40].

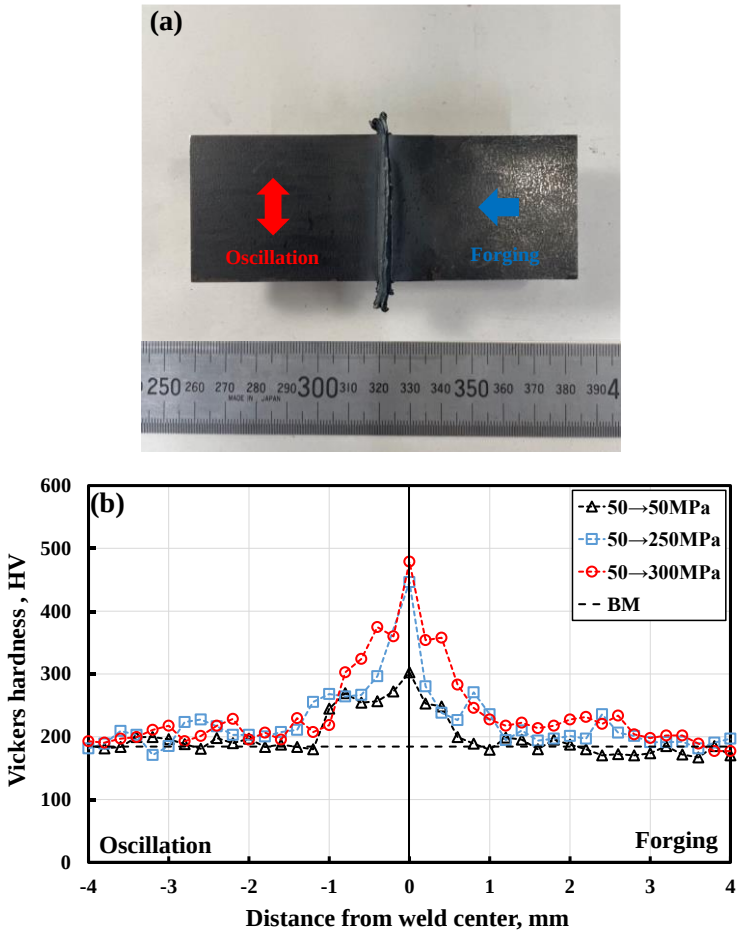

Fig. 5. (a) Appearance of 50→50MPa joint; (b) Hardness distribution of the LFW joints fabricated under various pressures after oscillation.

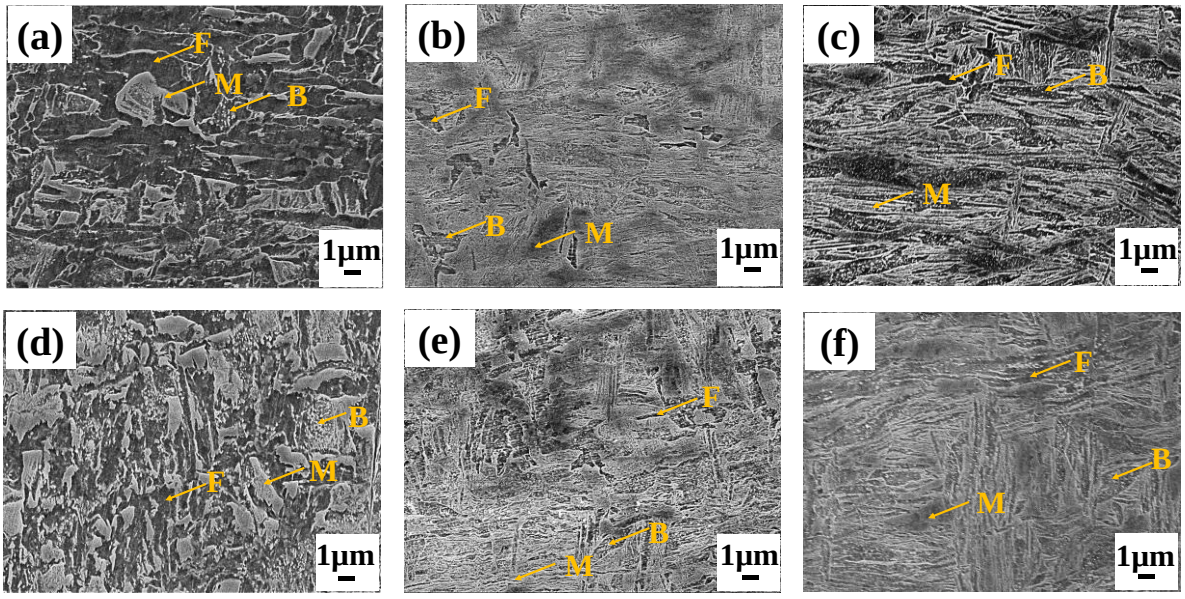

Fig. 6. SEM microstructures of middle and edges of the welding interface from the cross-section specimens under various pressures after oscillation: (a) 50→50MPa joint of center; (b) 50→250MPa joint of center; (c) 50→300MPa joint of center; (d) 50→50MPa joint of edge; (e) 50→250MPa joint of edge; (c) 50→300MPa joint of edge; F = ferrite, B = bainite and M = martensite.

3.2. Fatigue strength

A fatigue test was performed on the LFW joints fabricated under a constant final upset after pressurization. Fig. 7 shows the relationship between fatigue fracture life N_f and the nominal stress range $\Delta\sigma$ of the six LFW joints and three BM specimens. Furthermore, for comparison with the fatigue life of the LFW joints, the FAT90 design curve proposed by IIW [41] is plotted using a black diagonal line.

Because of the fatigue test, all LFW joints ruptured near the weld toe area, indicating that the welding conditions in this study achieved strong bonds at the weld interfaces. Importantly, the fatigue life of all the as-welded LFW joints greatly exceeded the FAT90 design curve, indicating that the LFW conditions in this study had sufficient fatigue strength, even when using as-welded joints with flash discontinuity. Under fatigue test conditions in the stress range of 380 MPa (maximum stress of 400 MPa), the fatigue life increased by approximately 31% when the pressure condition changed from 50→50MPa to 50→250MPa joints, The fatigue life improved by 87% when the pressure condition changed from 50→250MPa to 50→300MPa joints. In the conditions of the stress range of 332.5 MPa (maximum stress of 350 MPa). The fatigue life improved by 47% and 50% when the pressure condition changed from 50→50MPa to 50→250MPa and 50→300MPa joints, respectively. The fatigue life of the BM specimens were longer than those of the LFW joints.

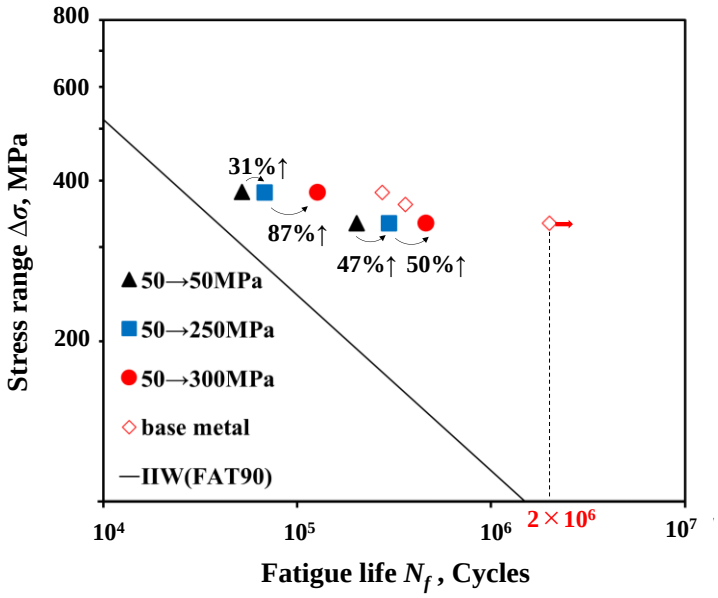

Fig. 7. The fatigue strength of LFW joints under various pressure conditions.

3.3. Fractography characteristics

In the fatigue test, all LFW joints fractured at the weld toe area**. Fig. 8** shows a fractograph of the LFW joint under the pressure condition of 50→50MPa. This fatigue test, conducted in the stress range of 380 MPa, is a representative example of the joint's appearance after fatigue testing. The LFW joints in this study were characterized by weld toe fractures, as indicated by the red arrow in Fig. 8. The strength of the welding interface was high and the sharp shape of the weld toe was prone to stress concentration compared to the welding interface. The current analysis was performed on a macroscopic scale, and it was proposed that the geometry of the weld toe affected the location of the fracture. However, past literature has suggested that the fracture could be ascribed to local concentrated dislocation movement at the weld toe, possibly presented as

stress or strain concentration [42]. In this study, the changes in the dislocations and microstructure at the weld toe were not investigated. Therefore, future studies should investigate the effects of these factors.

Fig. 9(a) shows a macro image of the fracture surface and the height distribution map of the fracture surface from the 50→50MPa joint under the fatigue condition of a stress range of 380 MPa. The fracture surface exhibited an evident height difference, characterized by crack propagation and ductile fracture regions with a fibrous pattern. The red dotted rectangle in Fig. 9(a) illustrates a possible area of fatigue crack initiation, exhibiting a quarter-circle characteristic of crack development near the weld edge. In **Fig. 9(b),** the SEM morphology of the crack propagation area in the quarter-circle region, as indicated by the red dotted line, shows typical striation associated with fatigue fractures. **Fig. 9(c)** reveals the fracture surface with large and deep dimples, a result of favorable ductility.

Fig. 10(a) shows a macro image of the fracture surface and the height distribution map of the fracture surface from the 50→300MPa joint under the fatigue condition at the stress range of 380 MPa. This fracture surface exhibited a significant height difference, characterized by crack propagation and a ductile fracture region with a fibrous pattern. **Fig. 10(b)** shows the SEM morphology of the crack propagation area indicated by the red dotted line, which indicates a typical striation characteristic of a fatigue fracture. **Fig. 10(c)** shows the joint center area and fatigue fracture surface, both showing the striation characteristics observed in the 50→300MPa joint. Therefore, the findings suggest that cracks propagate from the sides of the LFW joints, and the geometry of the weld toe is expected to be of importance.

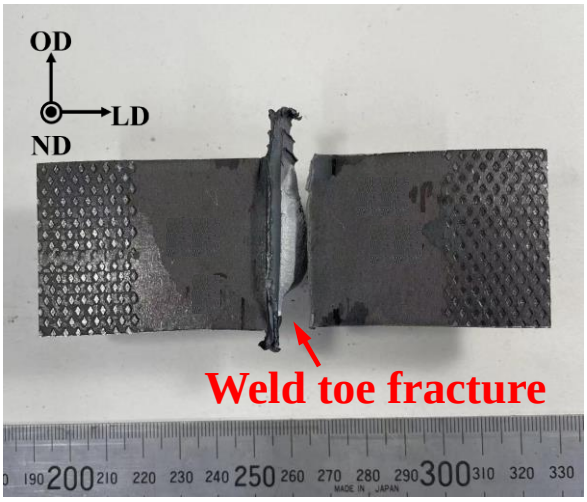

Fig. 8. Fractography characteristic of a weld toe fracture.

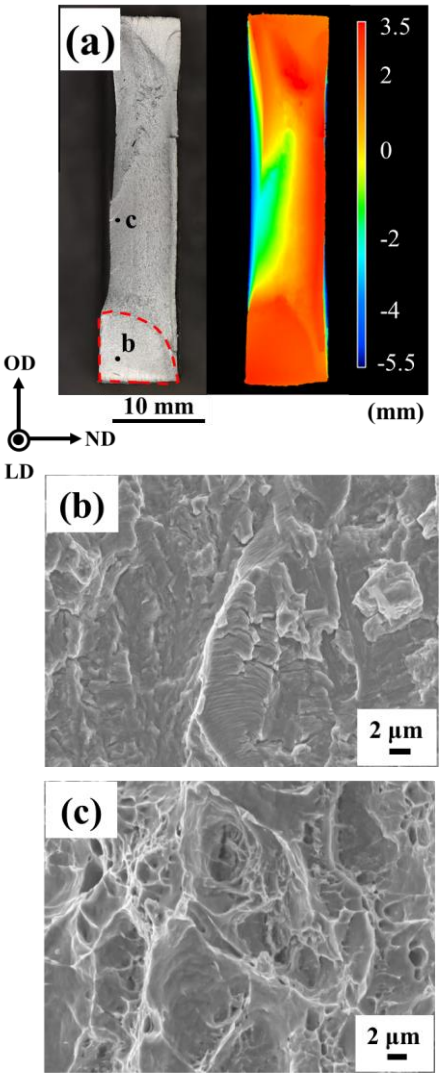

Fig. 9. Fractured surface morphology of 50→50MPa joint after fatigue test: (a) Fracture surfaces and height distribution of joint; (b)-(c) SEM observation of fracture surface ($\Delta\sigma$ = 380 MPa, N_f = 52,084, Red dotted line illustrated the fatigue fracture surface with striation).

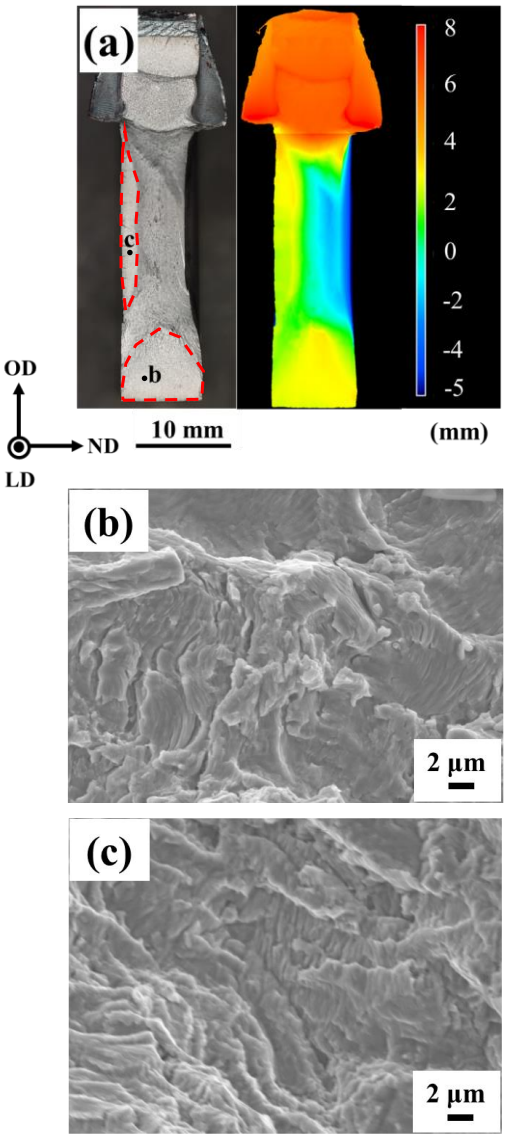

Fig. 10. Fractured surface morphology of 50→300MPa joint after fatigue test: (a) Fracture surfaces and height distribution of joint; (b)-(c) SEM observation of fracture surface ($\Delta\sigma$ = 380 MPa, N_f = 127,202, Red dotted line illustrated the fatigue fracture surface with striation).

4. Discussion

4.1. Reason for improved fatigue properties

Because the fracture position occurred at the weld toe, it was hypothesized that the change in the weld toe shape affected the fatigue properties. The weld toe profiles of the LFW joints were measured for joints welded under a constant final upset condition. The profile results for the 50→50MPa, 50→250MPa, and 50→300MPa joints are shown in **Fig. 11(a)–(c),** respectively. LFW flash typically exhibits a mountain-like shape, with the flash height and width near the edge of the joint being smaller than those near the center. Comparing the profiles of the 50→50MPa, 50→250MPa, and 50→300MPa joints, the height of the weld toe increased as the pressure increased. The maximum weld toe height increased from approximately 0 mm to 0.43 mm and 0.81 mm at the center of the specimen when the pressure was increased from 50 to 250 and 300 MPa, respectively. Next, the relationship between ρ and α obtained using the results of this profile measurement and the applied pressure are discussed.

Fig. 12(a) shows changes in ρ values plotted against the applied pressure after oscillation. The ρ value increased with the applied pressure after the oscillation, regardless of the measurement position. Specifically, the ρ value increased from 0.39 mm to 0.93 mm when the pressure after oscillation increased from 50 to 250 MPa. At the center, the ρ value reached a maximum value of 2.07 mm when the applied pressure after oscillation was 300 MPa. **Fig. 12(b)** shows the α values plotted against the applied pressure after oscillation**)**. The α value increased with increasing applied pressure after oscillation at each measurement point. For instance, α increased from 92.7° to 96.3° when the pressure after oscillation increased from 50 MPa to 250 MPa. Then, α showed a maximum value of 103.4° at the weld center with an applied pressure after oscillation of 300 MPa. The reason for the increase in α and ρ at the weld toe owing to higher pressure can be explained as follows: In LFW, the flow stress decreased as the welding temperature increased. Therefore, some of the welded specimens that could no longer withstand the applied pressure were deformed and discharged as flash. However, by increasing the pressure immediately after oscillation, the portion that was not deformed at a low applied pressure was deformed. This suggests that the values of α and ρ increased as the area of deformation expanded with higher applied pressure.

The size and shape of the weld toe can significantly affect the stress concentration and, hence, the fatigue strength of the welded joint. In particular, a small radius or sharp angle at the weld toe, i.e., small α and ρ values, can result in a high stress concentration factor (SCF), which can lead to lower fatigue strength. The K_t values were calculated using the formula for butt-welded joints loaded under tension proposed by Kiyak et al. [43]. K_t was calculated using the results from the center and both ends of the specimen at a total of three locations. **Fig. 13** shows the K_t values of the center and edges plotted against the applied pressure after oscillation. The K_t value decreased from 3.0 to 2.2 at the weld center when the pressure after oscillation increased from 50 MPa to 250 MPa. Then the K_t value decreased from 2.2 to 1.7 when the pressure after oscillation was increased from 250 to 300 MPa. The center of the specimen has a lower K_t value compared to each edge side of the specimen owing to the larger values of α and ρ in the center (see Fig. 12(a) and (b)). Therefore, it can be inferred that the fatigue properties of LFW joints can be improved by increasing the applied pressure after oscillation, smoothing the weld toe shape, and decreasing the stress concentration. However, the microstructural distribution of the weld toe and the residual stress distribution may affect the fatigue strength. Therefore, these factors should be investigated in future studies.

Fig. 14 shows a schematic of the weld toe shape change between constant pressure in the normal case and high pressure after the oscillation. In the oscillation stage, a low pressure with oscillation could achieve a high temperature at the welding interface for both the constant- and high-pressure cases. The weld toe shapes were almost the same before and after the forging pressure was applied in the constant pressure case.

However, in this study, high pressure was immediately applied to the welding interface at high temperatures after the oscillation. Therefore, a deformation area was induced between the BM and welding interface compared to the constant-pressure case. This deformation made the α and ρ increase significantly. As a result, this improved modification of the weld toe decreased the SCF and stress on the weld toe, thereby improving the fatigue strength.

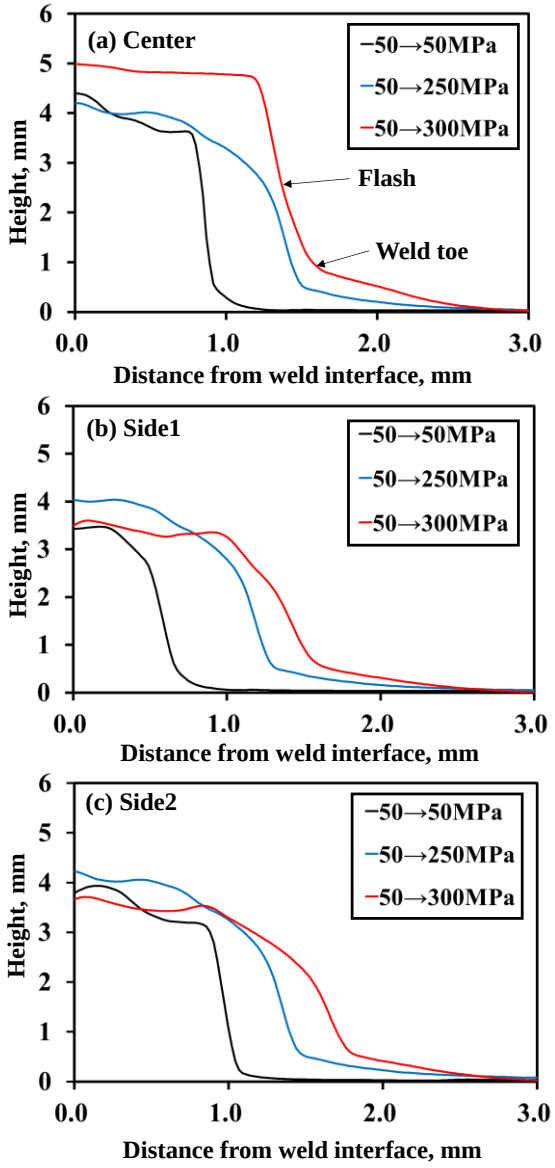

Fig. 11. Geometry profiles of welds under various pressure conditions after oscillation at a constant final upset after pressurizing (a) Center; (b) Side1; (c) Side2.

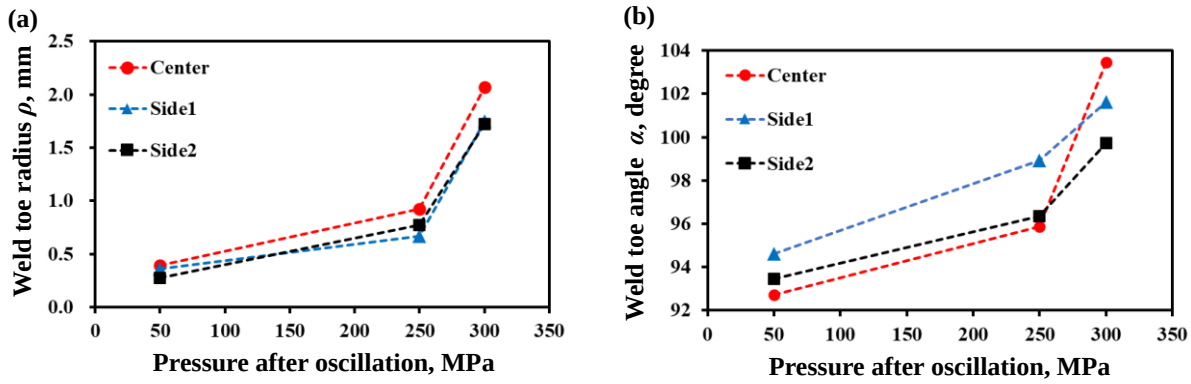

Fig. 12. Geometry characteristics for various pressures after oscillation under a constant final upset controlling method: (a) Weld toe radius; (b) Weld toe angle.

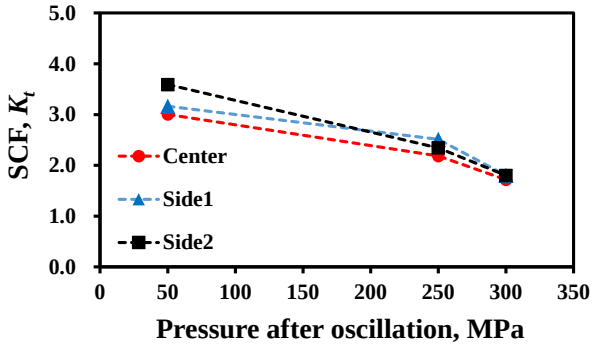

Fig. 13. The relation between pressures after oscillation and stress concentration factor under the upset control method of constant final upset after pressurizing.

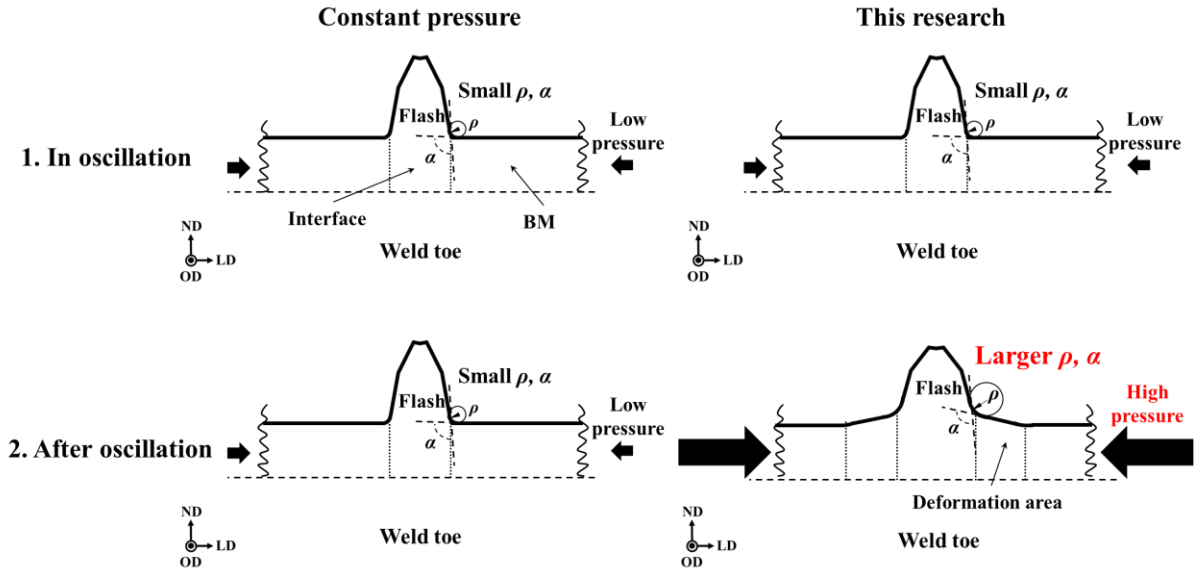

Fig. 14. Schematic of weld toe shape change between constant pressure in the normal case and high pressure after oscillation of this research.

4.2. Effect of upset control conditions on the weld toe shape

It was confirmed that increasing the applied pressure could increase the ρ and α at the weld toe, potentially leading to improved fatigue properties because of maintaining the SCF at a low value. In the joints where the fatigue properties were investigated, the final upset was maintained constant. However, changes in the upset during oscillation were ignored. Therefore, the investigation focused on the variation in upset during oscillation concerning the shape of the weld toe of LFW.

The profile results of the 50→50MPa, 50→250MPa, and 50→300MPa joints are presented in **Fig. 15(a)–(c)** under the constant-oscillation upset condition. The maximum height of weld toes increased from approximately 0.08 mm to 0.41 mm when the pressure after oscillation changed from 50 to 250 MPa. At the maximum pressure of 300 MPa, the maximum height of the weld toe was 0.72 mm at the center. **Fig. 16(a)** shows a graph plotting ρ against pressure after oscillation. Higher pressure after oscillation led to a higher ρ value at every measurement position of the joints. The ρ values increased from 0.31 mm to 0.90 mm when the pressure after oscillation increased from 50 to 250 MPa. The ρ values increased from 0.90 mm to 2.07 mm at the center of the specimen when the pressure after oscillation increased from 250 MPa to 300 MPa. Furthermore, the ρ showed a larger value at the weld center compared to the weld edges. **Fig. 16(b)** shows a plot of α against pressure after the oscillation. The α values increased in both the center and edge regions with increasing pressure after oscillation. At the weld center, α increased from 92.7° to 95.9° when the pressure after oscillation increased from 50 to 250 MPa. The α values of the center increased from 95.9° to 103.4° when the pressure after oscillation increased from 250 MPa to 300 MPa. Furthermore, the α values of the center were initially smaller than those of the edges at 50 and 250 MPa. However, when the pressure after oscillation increased to 300 MPa, the α of the center increased significantly.

Fig. 17 shows the changes in K_t values under the constant-oscillation upset condition as a function of the applied pressure. Additionally, the figure includes a white plot representing the K_t values when the final upset is maintained constant. The K_t value decreased from 3.4 to 2.2 at the weld center when the pressure after oscillation increased from 50 MPa to 250 MPa. At an applied pressure of 300 MPa after oscillation, the K_t value reached its smallest value of 1.7. The center of the specimen exhibited a lower K_t value compared to each edge side, primarily attributed to the larger values of α and ρ in the center (see Fig. 15(a) and (b)). The value of K_t was slightly smaller when the upset during oscillation was constant compared to when the final upset was constant at 50 MPa after oscillation. However, no significant difference was confirmed for all the pressure conditions. Considering that the values of α and ρ were nearly the same when compared, it can be inferred that the value of the upset during oscillation and the total amount of upset had little effect on the shape of the weld toe. Instead, it is believed that the pressure applied after the oscillation had a significant effect on the shape of the weld toe. The greater the pressure after oscillation, the greater the amount of plastic deformation (= value of final upset – the value of upset during oscillation) when the pressure is applied. Consequently, it is presumed that higher pressure leads to more material being ejected outward. Therefore, when using LFW for joining, one of the most effective methods to improve the fatigue properties is to increase the pressure after oscillation to alter the shape of the weld toe.

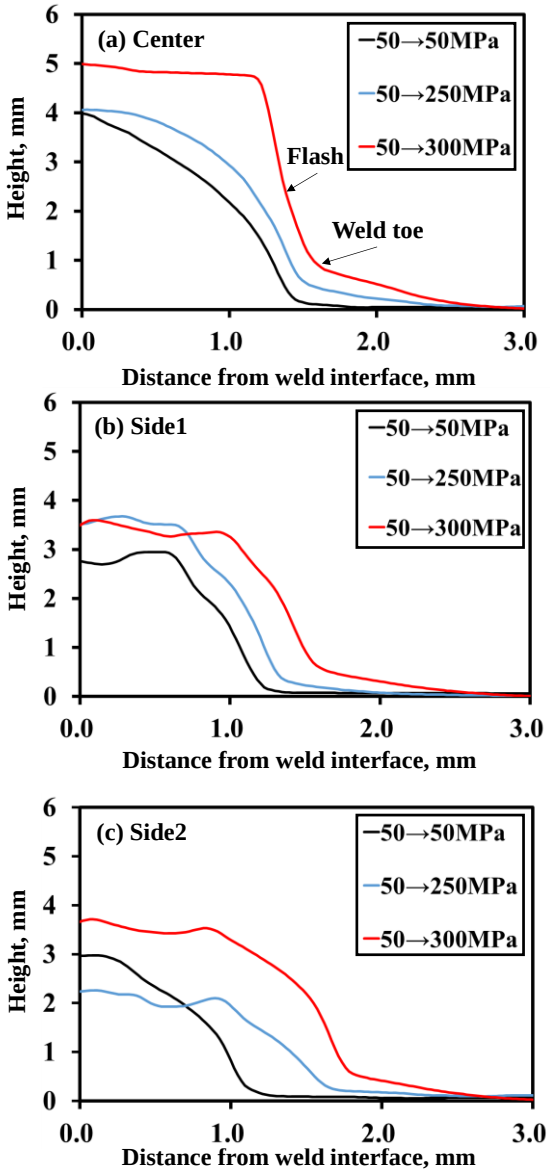

Fig. 15. Geometry profiles of welds under various pressure conditions after oscillation at a constant upset during oscillation (a) Center; (b) Side1; (c) Side2.

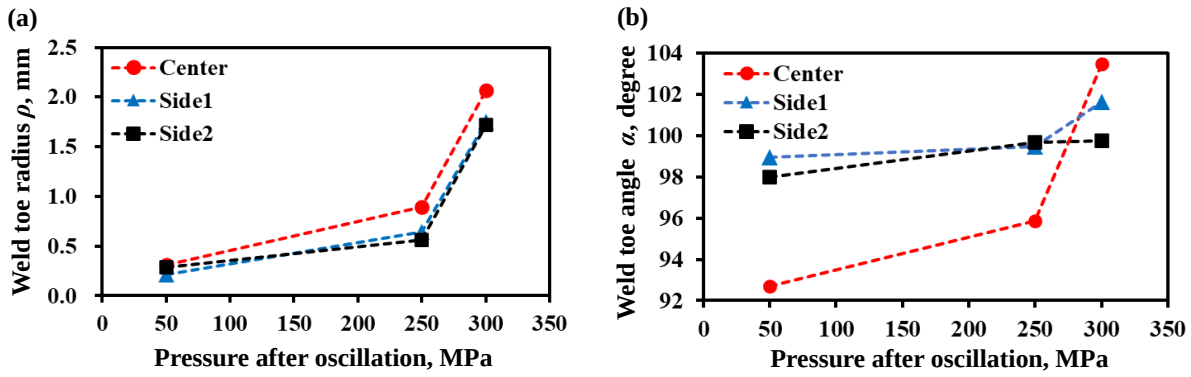

Fig. 16. Geometry characteristics for various pressures after oscillation at a constant upset during oscillation: (a) Weld toe radius; (b) Weld toe angle.

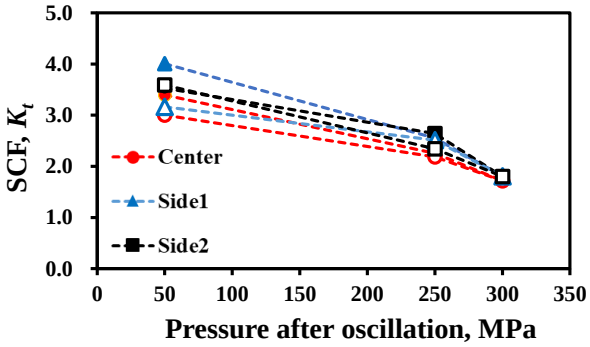

Fig. 17. The relation between pressures after oscillation and stress concentration factor under the upset control methods of constant upset during oscillation (The white plotted marks are results of constant final upset condition for comparison).

5. Conclusions

In this study, a butt configuration of 9 mm thick low carbon steel SM490A was successfully joined using LFW at different pressures after oscillation. The investigation focused on hardness, microstructure, weld toe profile, fatigue properties, and fracture behavior. The following conclusions were drawn:

(1) Increasing the pressure after oscillation from 50 MPa to 250 MPa and 300 MPa resulted in a more significant M fraction and a higher hardness value at the weld interface. However, no noticeable HAZ softening was observed for any of the LFW joints.

(2) The fatigue life of the LFW as-welded joints significantly improved from approximately 31% to 87% under the stress range of 380 MPa when the pressure after oscillation was increased from 50 MPa to 250 MPa and 300 MPa, respectively. All the joints demonstrated higher fatigue strength compared to the FAT90 design curve proposed by the IIW.

(3) All the LFW as-welded joints in this study displayed weld toe fractures. The fracture surface exhibited an evident height difference, characterized by crack propagation and ductile fracture regions with a fibrous pattern. Notably, a possible fatigue crack initiation area was identified on the weld edge, which could experience high stress levels owing to a higher stress concentration.

(4) The enhancement in fatigue strength of the LFW as-welded joints can be primarily attributed to the low K_t caused by the smoothing of the weld toe. The larger ρ and α values caused by the larger pressure after the oscillation led to a smaller K_t value, consequently lowering the stress level on the weld toe during the fatigue test.

(5) The larger ρ, α, and smaller K_t values were obtained by increasing the pressure after oscillation from 50 MPa to 250 MPa and 300 MPa, independent of the upset controlling conditions. Therefore, the primary reason for the change in the weld shape can be attributed to the pressure value after oscillation.

Caption list

Table 1 Chemical composition of low carbon steel (wt.%).

Table 2 LFW conditions of this study.

Fig. 1. SEM micrograph of the BM.

Fig. 2. Appearance of the equipment for the LFW and schematic illustration of the specimen.

Fig. 3. Schematic illustrations: (a) Sampling of microstructure observation and hardness test; (b) Fatigue specimens for the BM.

Fig. 4. (a) Definition of weld toe radius and weld toe angle, the horizontal line is parallel line of measurement; (b) Measurement locations for the weld toe shape.

Fig. 5. (a) Appearance of 50→50MPa joint; (b) Hardness distribution of the LFW joints fabricated under various pressures after oscillation.

Fig. 6. SEM microstructures of middle and edges of the welding interface from the cross-section specimens under various pressures after oscillation: (a) 50→50MPa joint of center; (b) 50→250MPa joint of center; (c) 50→300MPa joint of center; (d) 50→50MPa joint of edge; (e) 50→250MPa joint of edge; (c) 50→300MPa joint of edge; F = ferrite, B = bainite and M = martensite.

Fig. 7. The fatigue strength of LFW joints under various pressure conditions.

Fig. 8. Fractography characteristic of a weld toe fracture.

Fig. 9. Fractured surface morphology of 50→50MPa joint after fatigue test: (a) Fracture surfaces and height distribution of joint; (b)-(c) SEM observation of fracture surface ($\Delta\sigma$ = 380 MPa, N_f = 52,084, Red dotted line illustrated the fatigue fracture surface with striation).

Fig. 10. Fractured surface morphology of 50→300MPa joint after fatigue test: (a) Fracture surfaces and height distribution of joint; (b)-(c) SEM observation of fracture surface ($\Delta\sigma$ = 380 MPa, N_f = 127,202, Red dotted line illustrated the fatigue fracture surface with striation).

Fig. 11. Geometry profiles of welds under various pressure conditions after oscillation at a constant final upset after pressurizing (a) Center; (b) Side1; (c) Side2.

Fig. 12. Geometry characteristics for various pressures after oscillation under a constant final upset controlling method: (a) Weld toe radius; (b) Weld toe angle.

Fig. 13. The relation between pressures after oscillation and stress concentration factor under the upset control method of constant final upset after pressurizing.

Fig. 14. Schematic of weld toe shape change between constant pressure in the normal case and high pressure after oscillation of this research.

Fig. 15. Geometry profiles of welds under various pressure conditions after oscillation at a constant upset during oscillation (a) Center; (b) Side1; (c) Side2.

Fig. 16. Geometry characteristics for various pressures after oscillation at a constant upset during oscillation: (a) Weld toe radius; (b) Weld toe angle.

Fig. 17. The relation between pressures after oscillation and stress concentration factor under the upset control methods of constant upset during oscillation (The white plotted marks are results of constant final upset condition for comparison).

Declaration of Competing Interest

The authors report no declarations of interest.

Acknowledgments

This work was supported in part by the JST SPRING (Grant Number JPMJSP2138) and a grant-in-aid for scientific research from the Japan Society for the Promotion of Science (19H00826).

References

[1] Matsuda T, Adachi H, Yoshida R, Sano T, Hori H, Hirose A. Formation of interfacial reaction layer for stainless steel/aluminum alloy dissimilar joint in linear friction welding. Mater Today Commun 2021;26. https://doi.org/10.1016/j.mtcomm.2020.101700.

[2] Zhao P, Tao Y, Chen H, et al. Texture characteristics and fracture mechanism of linear friction welded joints of dissimilar titanium alloys after annealing. Mater Sci Eng A 2023;866:144709. https://doi.org/10.1016/j.msea.2023.144709.

[3] Geng P, Qin G, Ma H, Zhou J, Ma N. Linear friction welding of dissimilar Ni-based superalloys: Microstructure evolution and thermo-mechanical interaction. J Mater Res Technol 2021;11:633-649. https://doi.org/10.1016/j.jmrt.2021.01.036.

[4] Choi JW, Aoki Y, Ushioda K, Fujii H. Effect of the welding parameters on microstructure and mechanical properties of linear friction welded Ti-6Al-4V alloy. J Manuf Process 2022;75:651-663. https://doi.org/10.1016/j.jmapro.2022.01.033.

[5] Choi JW, Aoki Y, Ushioda K, Fujii H. Linear friction welding of Ti-6Al-4V alloy fabricated below β-phase transformation temperature. Scr Mater 2021;191:12-16. https://doi.org/10.1016/j.scriptamat.2020.09.013.

[6] Li WY, Ma T, Li J. Numerical simulation of linear friction welding of titanium alloy: Effects of processing parameters. Mater Des 2010;31(3): 1497–1507. https://doi.org/10.1016/j.matdes.2009.08.023.

[7] Vairis A, Frost M. Modelling the linear friction welding of titanium blocks. Mater Sci Eng A 2000;292: 8-17. https://doi.org/www.elsevier.com/locate/msea doi.

[8] Kuroiwa R, Liu H, Aoki Y, Yoon S, Fujii H, Murayama G, Yasuyama M. Microstructure control of medium carbon steel joints by low-temperature linear friction welding. Sci Technol Weld 2020;25(1): 1–9. https://doi.org/10.1080/13621718.2019.1600771.

[9] Dalgaard E, Wanjara P, Gholipour J, Cao X, Jonas JJ. Linear friction welding of a near-β titanium alloy. Acta Mater. 2012;60: 770–780. https://doi.org/10.1016/j.actamat.2011.04.037.

[10] Wanjara P, Jahazi M. Linear friction welding of Ti-6Al-4V: processing, microstructure, and mechanical property inter-relationships. Metall Mater Trans A. 2005;36: 2149–2164. https://doi.org/10.1007/s11661-005-0335-5.

[11] Vairis A, Frost M. Modelling the linear friction welding of titanium blocks. Mater Sci Eng A. 2000;292: 8–17. https://doi.org/10.1016/S0921-5093(00)01036-4.

[12] Kimura M, Choji M, Kusaka M, Seo K, Fuji A. Sci. Technol. Weld. Join., 10 (2005), 406. https://doi.org/10.1179/174329305X44125.

[13] Bhamji I, Preuss M, Threadgill PL, Addison AC. Solid state joining of metals by linear friction welding: A literature review. Mater Sci Technol 2011;27(1): 2–12. https://doi.org/10.1179/026708310X520510.

[14] Chamanfar A, Jahazi M, Cormier J. A review on inertia and linear friction welding of Ni-based superalloys. Metall Mater Trans A Phys Metall Mater Sci 2015;46(4): 1639–1669. https://doi.org/10.1007/s11661-015-2752-4.

[15] McAndrew AR, Colegrove PA, Bühr C, Flipo BCD, Vairis A. A literature review of Ti-6Al-4V linear friction welding. Prog Mater Sci 2018;92: 225–257. https://doi.org/10.1016/j.pmatsci.2017.10.003.

[16] Turner R, Gebelin JC, Ward RM, Reed R C. Linear friction welding of Ti-6Al-4V: Modelling and validation. Acta Mater 2011;59(10): 3792–3803. https://doi.org/10.1016/j.actamat.2011.02.028.

[17] Geng P, Qin G, Zhou J. Computational investigation of welding heat transfer characteristics and parameters effectiveness in mild steel linear friction welding. *J Manuf Process* 2020;49: 234-246. https://doi:10.1016/j.jmapro.2019.11.023.

[18] Kelly MR, Schmid SR, Adams DC, Fletcher J, Heard R. Experimental investigation of linear friction welding of AISI 1020 steel with pre-heating. *J Manuf Process* 2019;39:26-39. https://doi:10.1016/j.jmapro.2019.01.038

[19] Nakashima M, Inoue K, Tada M. Classification of damage to steel buildings observed in the 1995 Hyogoken-Nanbu earthquake. Eng Struct 1998;20(4-6): 271–81. https://doi.org/10.1016/S0141-0296(97)00019-9.

[20] Owsiński R, Lachowicz DS, Lachowicz CT, Gil R, Niesłony A. Characterisation of joint properties through spatial mapping of cracks in fatigue specimens, extracted from the linear friction welded steel coupon. Precis Eng 2021;71: 78–89. https://doi.org/10.1016/j.precisioneng.2021.02.008.

[21] Kuroki H, Kondo Y, Wakabayashi T, Nakamura K, Takamatsu K, Nezaki K, Tsunori M. Fatigue characteristic of linear friction welded Ti-6Al-4V joints. LNME 2020; 3–15. https://doi.org/10.1007/978-3-030-21503-3_1.

[22] Stinville JC, Bridier F, Ponsen D, Wanjara P, Bocher P. High and low cycle fatigue behavior of linear friction welded Ti-6Al-4V. Int J Fatigue 2015;70: 278–288. https://doi.org/10.1016/j.ijfatigue.2014.10.002.

[23] Wen GD, Ma TJ, Li WY, Wang SQ, Guo HZ, Chen DL. Strain-controlled fatigue properties of linear friction welded dissimilar joints between Ti-6Al-4V and Ti-6.5Al-3.5Mo-1.5Zr-0.3Si alloys. Mater Sci Eng A 2014;612: 80–88. https://doi.org/10.1016/j.msea.2014.06.010.

[24] Wang Y, Tsutsumi S, Kawakubo T, Fujii H. Microstructure, mechanical properties and fatigue behaviors of linear friction welded weathering steels. Int J Fatigue 2022;159. https://doi.org/10.1016/j.ijfatigue.2022.106829.

[25] Wang Y, Tsutsumi S, Kawakubo T, Fujii H. Fatigue strength and fracture characteristics of linear friction welded joints of weathering mild steel. Fatigue Fract Eng Mater Struct 2022;45(10): 2769–2783. https://doi.org/10.1111/ffe.13772.

[26] Kang G, Luo H. Review on fatigue life prediction models of welded joint. Acta Mech Sin Xuebao 2020;36(3):701–26. https://doi.org/10.1007/s10409-020-00957-0.

[27] Lee JH, Park SH, Kwon HS, Kim GS, Lee CS. Laser, tungsten inert gas, and metal active gas welding of DP780 steel: Comparison of hardness, tensile properties and fatigue resistance. *Mater Des*. 2014; 64:559-565. https://doi.org/10.1016/j.matdes.2014.07.065.

[28] Tanaka K, Nishijima S, Matsuoka S, Abe T, Kouzu F. Low-and high-cycle fatigue properties of various steels specified in JIS for machine structural use. Fatigue & Fracture of Engineering Materials & Structures 1981;4:97-108. https://doi.org/10.1111/j.1460-2695.1981.tb01377.x

[29] Sherman AM, Davies RO. Influence of Martensite Carbon Content on the Cyclic Properties of Dual-Phase Steel.1981; 3(4): 195-198. https://doi.org/10.1016/0142-1123(81)90020-7.

[30] Dai W, Yao Z, Zhang H, Li C, Liu Y, Zhang Y. Effect of forging ratio on tensile properties and fatigue performance of EA4T steel. *J Manuf Process* 2022;76:291-303. https://doi:10.1016/j.jmapro.2022.02.026.

[31] Wang DQQ, Yao DD, Wang Q, Gao ZB, Zhang ZF, Li XW. Evaluating the fatigue property of S355J2W steel butt-welded joint: Multiple notch effects. *Int J Fatigue*. 2023;167. https://doi.org/10.1016/j.ijfatigue.2022.107362.

[32] Lazzarin P, Lassen T, Livieri P. A notch stress intensity approach applied to fatigue life predictions of welded joints with different local toe geometry. *Fatigue Fract Eng Mater Struct*. 2003;26(1):49-58. https://doi.org/10.1046/j.1460-2695.2003.00586.x.

[33] Remes H, Varsta O. Statistics of weld geometry for laser-hybrid welded joints and its application within notch stress approach. *Welding in the World. 2010*; 54:R189-R207. https://doi.org/10.1007/BF03263505.

[34] Ye N, Moan T. Improving fatigue life for aluminum cruciform joints by weld toe grinding. Fatigue Fract Eng Mater Struct 2008;31(2): 152–63. https://doi.org/10.1111/j.1460-2695.2007.01210.x.

[35] Tateishi K, Hanji T, Hanibuchi S. Improvement of extremely low cycle fatigue strength of welded joints by toe finishing. Weld World 2009;53(9-10):R238–45. https://doi.org/10.1007/BF03321135.

[36] Yildirim HC. Review of fatigue data for welds improved by tungsten inert gas dressing. Int J Fatigue 2015;79:36–45. https://doi.org/10.1016/j. ijfatigue.2015.04.017.

[37] Luo Y, Ma R, Tsutsumi S. Parametric formulae for elastic stress concentration factor at the weld toe of distorted butt-welded joints. *Materials*. 2020;13(1). https://doi.org/10.3390/ma13010169

[38] Yonekura K, Shinohara T, Masaki K. Cost-effective estimation of flash extrusion and defects in linear friction welding using Voronoi diagrams. *J Manuf Process* 2021;68:158-167. https://doi:10.1016/j.jmapro.2021.07.012.

[39] Wang C, Guo Q, Zhu X, et al. Effect of post-weld heat treatment on microstructure and property of linear friction welded TC17/TA15 titanium alloy joint. *Mater Charact*. Published online May 2023;112799. https://doi.org/10.1016/j.matchar.2023.112799.

[40] Asadi M, de Cooman BC, Palkowski H. Influence of martensite volume fraction and cooling rate on the properties of thermomechanically processed dual phase steel. Mater Sci Eng A 2012;538:42–52. https://doi.org/10.1016/j.msea.2012.01.010.

[41] Hobbacher AF. IIW collection recommendations for fatigue design of welded joints and components. Springer 2016.

[42] Guo Z, Ma T, Yang X, et al. In-situ investigation on dislocation slip concentrated fracture mechanism of linear friction welded dissimilar Ti17(α+β)/Ti17(β) titanium alloy joint. *Materials Science and Engineering: A* 2023;872. https://doi:10.1016/j.msea.2023.144991

[43] Kiyak Y, Madia M, Zerbst U. Extended parametric equations for weld toe stress concentration factors and through-thickness stress distributions in butt-welded plates subject to tensile and bending loading. Weld World 2016;60:1247–1259. https://doi.org/10.1007/s40194-016-0377-x.